Research Article | Vol. 30, No. 20 / 26 Sep 2022 / Optics Express 36464
Optics EXPRESS

High-fidelity temporally-corrected transmission through dynamic smoke via pixel-to-plane data encoding

YONGGUI CAO,[1] YIN XIAO,[1] ZILAN PAN,[1] LINA ZHOU,[1] AND WEN CHEN[1,2,*]

[1]Department of Electronic and Information Engineering, The Hong Kong Polytechnic University, Hong Kong, China
[2]Photonics Research Institute, The Hong Kong Polytechnic University, Hong Kong, China
*owen.chen@polyu.edu.hk

Abstract: We propose a new approach for high-fidelity free-space optical data transmission through dynamic smoke using a series of 2D arrays of random numbers as information carriers. Data to be transmitted in dynamic smoke environment is first encoded into a series of 2D arrays of random numbers. Then, the generated 2D arrays of random numbers and the fixed reference pattern are alternately embedded into amplitude-only spatial light modulator, and are illuminated to propagate through dynamic smoke in free space. Real-time optical thickness (OT) is calculated to describe temporal change of the properties of optical wave in dynamic smoke environment, and transmission noise and errors caused by dynamic smoke are temporally suppressed or corrected. Optical experiments are conducted to analyze the proposed method using different experimental parameters in various scenarios. Experimental results fully verify feasibility and effectiveness of the proposed method. It is experimentally demonstrated that irregular analog signals can always be retrieved with high fidelity at the receiving end by using the proposed method, when average optical thickness (AOT) is lower than 2.5. The proposed method also shows high robustness against dynamic smoke with different concentrations. The proposed method could open up an avenue for high-fidelity free-space optical data transmission through dynamic smoke.

1. Introduction

With ever-growing popularity of wireless communication, radio-frequency (RF) technologies and systems are widely deployed and utilized in our community [1,2]. The RF band of electromagnetic spectrum is expensive and fundamentally limited in capacity, since most sub-bands are exclusively licensed [3]. It is desirable and crucial to consider other options for wireless communication that rely on other electromagnetic spectra. Compared with traditional RF technologies, free-space optical communication has attracted much increasing attention in recent years due to its free and abundant spectrum resources, low power consumption and low cost [3,4]. Free-space optical data transmission often encounters absorption and scattering phenomena due to atmospheric conditions. In fact, optical transmission or imaging [5–7] through scattering media, e.g., smoke, rain, fog and dust, is always regarded as a significant challenge due to the severely degrading of optical field information. To verify the free-space optical data transmission, much research work has been conducted using different light sources in various optical transmission environments, e.g., atmospheric conditions [8–11] and underwater [12,13].

In atmospheric environments, smoke or fog severely attenuates the propagating light and degrades signal-to-noise ratio (SNR) of transmitted signals. When the light beam propagates through smoke or fog, light intensities [14–21], optical polarization states [22–27] and optical field information [28,29] could be changed. In particular, atmospheric environments, e.g., smoke, always have a dynamic property as a result of the changeable meteorological conditions. Due

#469930 https://doi.org/10.1364/OE.469930
Journal © 2022 Received 6 Jul 2022; revised 30 Aug 2022; accepted 31 Aug 2022; published 21 Sep 2022

Optics EXPRESS

to the settlement and liquefaction of smoke, the properties of optical field information could be dynamically changed during optical data transmission. Therefore, temporal changes of dynamic smoke affect the transmission and detection of optical information, and optical data information collected at the receiving end always contains large transmission errors. Performance of free-space optical communication can be severely impaired by the absorption, scattering, and dynamic change of smoke properties. However, optical experiments [30–32] are mainly aimed to study the effect of different channel properties [32] of smoke environment on the transmission rate. Many methods [33–36] have also been developed to mitigate the transmission error caused by atmospheric turbulence. For instance, decision feedback equalizer [34] optimized by minimum mean square error was investigated to improve performance of optical communication in various atmospheric conditions. However, few studies have been conducted on optical data transmission through dynamic smoke. In fact, free-space optical analog-signal transmission in a dynamic smoke environment is challenging, and it is highly desirable to investigate the influence of dynamic smoke environment on free-space optical analog-data transmission.

In this paper, high-fidelity free-space optical data transmission through dynamic smoke is studied by using a pixel-to-plane encoding algorithm to generate a series of 2D arrays of random numbers as information carriers. A novel pixel-to-plane encoding algorithm is first developed to generate 2D arrays of random numbers constrained by each pixel of the signal to be transmitted. To eliminate transmission errors caused by dynamic smoke, a fixed reference pattern is further introduced and used to conduct dynamic compensation, and transmission errors and noise induced by dynamic smoke are temporally corrected. Experimental results are obtained to verify the proposed method, when the developed free-space optical data transmission scheme is applied in dynamic smoke environment with different concentrations. It is demonstrated that irregular analog signals can always be retrieved with high fidelity at the receiving end after transmitting through dynamic smoke. Moreover, the proposed method also shows high robustness against dynamic smoke with different concentrations. The proposed method could open up a new research perspective for free-space optical data transmission through dynamic smoke.

2. Principle

A series of 2D arrays of random numbers are first generated as information carriers in the proposed method to realize high-fidelity free-space optical data transmission through dynamic smoke. In the proposed method, a sequence of pixels of the signal (S_i, $i = 1,2,3,\ldots,N$) to be transmitted are encoded into a series of 2D arrays of random numbers, and the data encoding procedure is as follows:

(1) An enlarged value MS_i is obtained by a multiplication between each pixel value S_i and a given magnification factor M.

(2) A value T_i is calculated by using a subtraction operation between the enlarged value MS_i and the sum of a random matrix $\mathbf{P}_i$ with real and non-negative values, where the size of random matrix $\mathbf{P}_i$ is 512×512 pixels.

(3) The absolute value of T_i obtained in Step (2) contains two parts, i.e., an integer value m_i and a fractional part n_i respectively described by

$$m_i = int\{|T_i|\}, \tag{1}$$

$$n_i = dec\{|T_i|\}, \tag{2}$$

where $||$ denotes an absolute operation, m_i denotes integer part of $|T_i|$, and n_i denotes fractional part of $|T_i|$. Then, the integer value is divided into m_i pixels with each pixel value of 1, and the decimal value n_i (i.e., fractional part) remains to be only one pixel.

Optics EXPRESS

These pixels, i.e., m_i+1, are used to arbitrarily replace m_i+1 positions of a pre-generated all-zero matrix in order to generate matrix $\mathbf{F}_i$ with 512×512 pixels.

(4) A 2D array of random numbers corresponding to each pixel S_i of the signal is finally generated by

$$\hat{\mathbf{P}}_i = \begin{cases} \mathbf{P}_i + \mathbf{F}_i, & T_i \geq 0 \\ \mathbf{P}_i - \mathbf{F}_i, & T_i < 0 \end{cases}, \tag{3}$$

where $\hat{\mathbf{P}}_i$ denotes a generated 2D array of random numbers. To clearly illustrate the generation process, a flow chart is shown in Fig. 1.

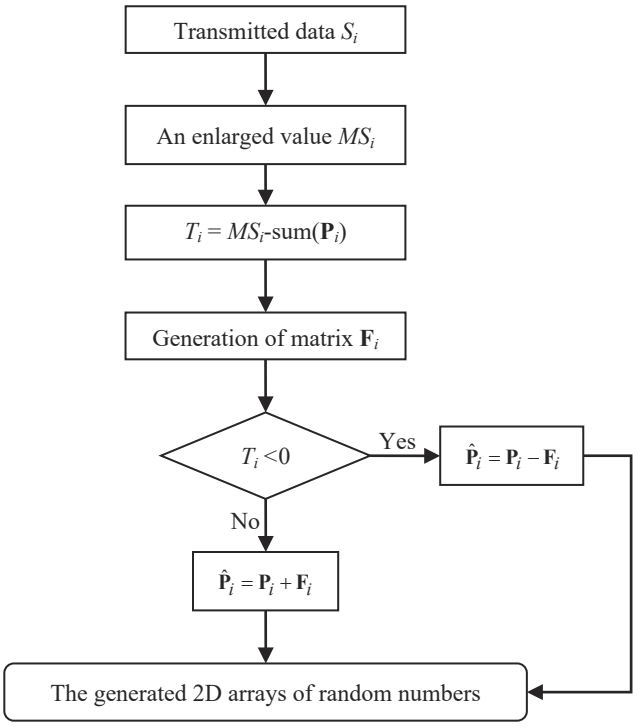

Fig. 1. A flow chart to illustrate the generation of 2D arrays of random numbers to encode the signal.

The magnification factor M used in Step (1) plays an important role in the proposed pixel-to-plane encoding algorithm, and it needs to satisfy that the enlarged value is comparable to the total number of pixels in the generated 2D array of random numbers. The size of 2D arrays of random numbers is 512×512 pixels in this study, and a typical magnification factor M of 1.0×10^5 can be used.

The 2D arrays of random numbers $\hat{\mathbf{P}}_i$ could be embedded into amplitude-only spatial light modulator in Fig. 2. According to wave propagation theory [37,38], light intensities collected by single-pixel bucket detector at the receiving end can be described by

$$\begin{aligned} b_i &= k \iint \hat{\mathbf{P}}_i(x,y) e^{-2\pi j(x\xi + y\eta)} dxdy|_{\xi=0,\eta=0} \\ &= k \iint \hat{\mathbf{P}}_i(x,y) dxdy \end{aligned}, \tag{4}$$

Optics EXPRESS

where (x,y) and (ξ,η) denote the coordinates, k denotes a scaling factor, and b_i denotes the recorded ith intensity value.

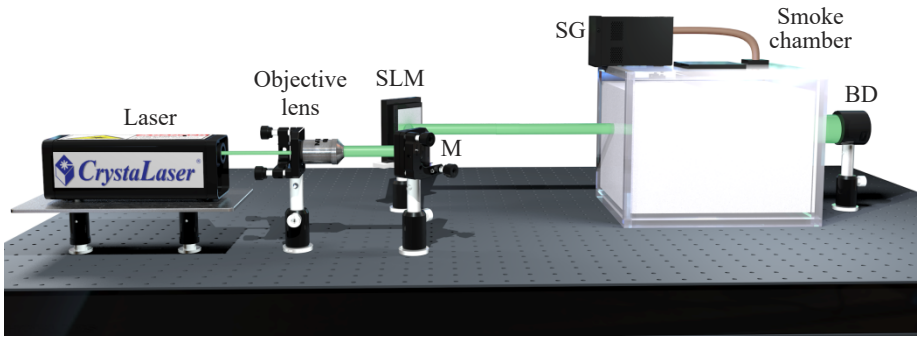

Fig. 2. A schematic experimental setup for the proposed free-space optical data transmission in a dynamic smoke environment: M, Mirror; SLM, Amplitude-only spatial light modulator; BD, Single-pixel bucket detector; SG, Smoke generator.

In Fig. 2, smoke is generated and pumped into a chamber to be considered as a dynamic smoke channel in free space, and liquefaction and sedimentation of smoke particles dynamically change scattering properties in the chamber. In the process of light intensity measurement, environmental and shot noise affects quality of the retrieved signals at the receiving end. To suppress noise, a differential operation is proposed and applied in this study. When all the pixel values of original signal to be transmitted are individually encoded into 2D arrays of random numbers ($\hat{\mathbf{P}}_i,\ i = 1, 2, 3, \ldots, N$) is further converted into two separate 2D arrays, i.e., $\mathbf{B} + \hat{\mathbf{P}}_i$ and $\mathbf{B} - \hat{\mathbf{P}}_i$ where $\mathbf{B}$ denotes a real and non-negative value.

Since dynamic smoke environment in Fig. 2 results in a loss or distortion of optical field information, a fixed reference pattern $\mathbf{R}$, i.e., a pre-generated random amplitude-only pattern, is used before each generated 2D array of random numbers (i.e., $\mathbf{B} + \hat{\mathbf{P}}_i$ and $\mathbf{B} - \hat{\mathbf{P}}_i$). Therefore, four 2D arrays of random numbers corresponding to each pixel of the transmitted signal need to be sequentially embedded into amplitude-only spatial light modulator in Fig. 2. The reference pattern [39,40] plays an important role in the proposed high-fidelity free-space optical data transmission scheme. Scaling factors physically existing in the free-space optical transmission channel dynamically change due to dynamic smoke, and the fixed reference pattern is introduced here and used to overcome this challenge. For instance, the reference pattern R is embedded into spatial light modulator at time slot t_i, and an intensity value b_{ir} is collected by using single-pixel bucket detector at the receiving end. Then, 2D array of random numbers ($\mathbf{B} + \hat{\mathbf{P}}_i$) is embedded into spatial light modulator at time slot t_{i+1}, and an intensity value b_{i1} is recorded. Subsequently, the fixed reference pattern R is embedded into spatial light modulator again at time slot t_{i+2}, and an intensity value $\tilde{b}_{ir}$ is recorded. Finally, the 2D array of random numbers ($\mathbf{B} - \hat{\mathbf{P}}_i$) is embedded into spatial light modulator at time slot t_{i+3}, and an intensity value b_{i2} is collected. For each pixel of the signal to be transmitted, the four recordings by using the single-pixel bucket detector can be respectively described by

$$b_{ir} \approx k(t_i) \iint \mathbf{R}(x, y)dxdy, \tag{5}$$

$$b_{i1} \approx k(t_{i+1}) \iint [\mathbf{B} + \hat{\mathbf{P}}_i(x, y)]dxdy, \tag{6}$$

$$\tilde{b}_{ir} \approx k(t_{i+2}) \iint \mathbf{R}(x, y)dxdy, \tag{7}$$

Optics EXPRESS

$$b_{i2} \approx k(t_{i+3}) \iint [\mathbf{B} - \hat{\mathbf{P}}_i(x, y)] dxdy, \tag{8}$$

where $k(t)$ denotes scaling factor at time slot t.

Since the time interval is short to display the patterns in amplitude-only spatial light modulator in each group of four measurements for optically transmitting each pixel of the signal, we have

$$k(t_i) \approx k(t_{i+1}), \tag{9}$$

$$k(t_{i+2}) \approx k(t_{i+3}). \tag{10}$$

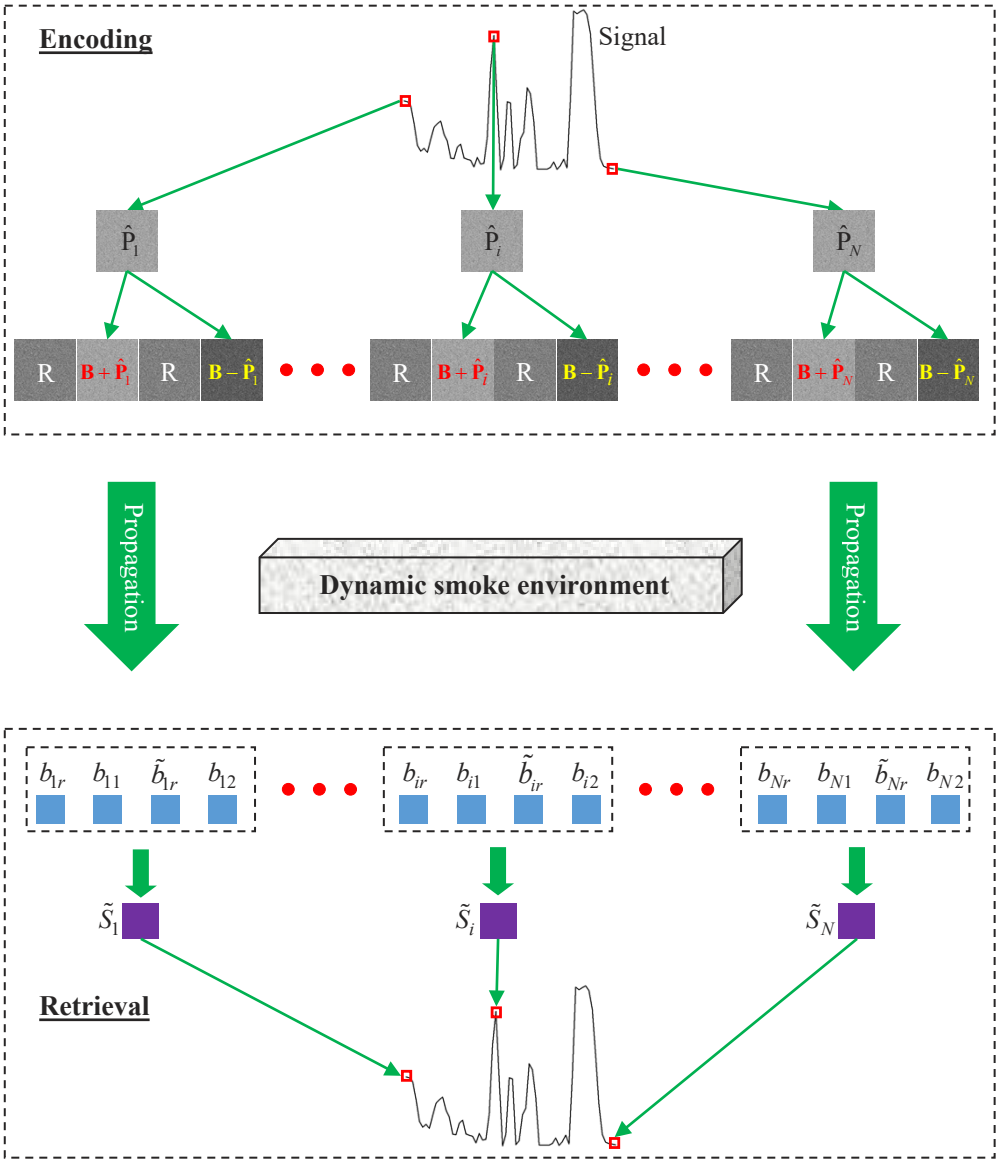

Fig. 3. A flow chart of the proposed high-fidelity free-space optical data transmission through dynamic smoke.

Optics EXPRESS

Therefore, a signal $\tilde{S}_i$ can be retrieved at the receiving end described by

$$\begin{aligned}\tilde{S}_i &= \frac{k(t_{i+1})\iint[\mathbf{B}+\hat{\mathbf{P}}_i(x,y)]dxdy}{k(t_i)\iint\mathbf{R}(x,y)dxdy} - \frac{k(t_{i+3})\iint[\mathbf{B}-\hat{\mathbf{P}}_i(x,y)]dxdy}{k(t_{i+2})\iint\mathbf{R}(x,y)dxdy} \\ &= \frac{1}{\iint\mathbf{R}(x,y)dxdy}\left\{\iint[\mathbf{B}+\hat{\mathbf{P}}_i(x,y)]dxdy - \iint[\mathbf{B}-\hat{\mathbf{P}}_i(x,y)]dxdy\right\}, \\ &= K\iint\hat{\mathbf{P}}_i(x,y)dxdy\end{aligned} \tag{11}$$

where K denotes scaling factor between the retrieved signal and original signal, which is described by

$$K = \frac{2}{\iint\mathbf{R}(x,y)dxdy}. \tag{12}$$

Therefore, based on Eq. (11), the proposed method is able to realize high-fidelity free-space optical data transmission through dynamic smoke. To clearly illustrate the proposed method, a flow chart is further shown in Fig. 3.

3. Experimental results and discussion

3.1. Experimental setup

To verify feasibility and effectiveness of the proposed method, a series of optical experiments are conducted, and a schematic experimental setup is shown in Fig. 2. An objective lens is used to expand a diode-pumped green laser (CrystaLaser, CL532-025-S) with a power of 25.0 mW and wavelength of 532.0 nm. The series of generated 2D arrays of random numbers and the fixed reference pattern are alternately embedded into an amplitude-only spatial light modulator (Holoeye, LC-R720) with pixel size of 20.0 μm to be illuminated by the collimated light. In optical experiments, refreshing rate of the spatial light modulator is set as 1.25 Hz as a typical example to illustrate the proposed method. Then, dynamic smoke is generated and pumped into an acrylic chamber placed in the beam path. The artificially-generated smoke is produced by using a commercial smoke generator (HALFSun, power of 3000W and pumping rate of 973.0 cm^3/s) and smoke oil. The smoke oil is a mixture of glycerol and water. Therefore, dynamic smoke environments are established. Light intensities after propagating through dynamic smoke are recorded by using a single-pixel bucket detector (Newport, 918D-UV-OD3R) without a front lens. Different from other free-space optical data transmission systems, a single-pixel bucket detector is used in the proposed method to collect light intensities at the receiving end. Finally, the recorded experimental data is demodulated to retrieve the transmitted signal using the proposed method.

To illustrate optical data transmission in optical experiments, axial distances are shown in Fig. 4. The axial distance between amplitude-only spatial light modulator and front side of smoke chamber is denoted as d_1, and the length of smoke chamber is denoted as d_2. The axial distance between back side of smoke chamber and single-pixel bucket detector is denoted as d_3. In optical experiments, the total axial transmission distance, i.e., $d_1 + d_2 + d_3$, is fixed at 105.0 cm. Other experimental parameters are given in Table 1. Acrylic chambers with different volumes (i.e., 20(L)×30(W)×40(H), $30\times30\times40$, $40\times30\times40$, $60\times30\times40$, $80\times30\times40$, and $100\times30\times40$ cm^3) are designed to conduct optical experiments for a comparison. Six lengths of d_2 in Fig. 4 are respectively used, i.e., 20.0, 30.0, 40.0, 60.0, 80.0 and 100.0 cm. In the smoke chambers, width and height of smoke chambers are fixed at 30.0 cm and 40.0 cm, respectively. The axial distance d_3 between back side of smoke chamber and single-pixel bucket detector is fixed at 2.5 cm. To generate smoke with the same concentration in the chamber with different volumes for a comparison, a fixed ratio of 0.3041 between the total smoke volume pumped into acrylic chamber and the total volume of acrylic chamber is employed. Dynamic smoke is produced into the acrylic chamber during free-space optical data transmission from top side of the chamber, as shown in

Optics EXPRESS

Fig. 2. Due to the existence of liquefaction and sedimentation of the smoke, smoke environment dynamically changes during optical experiments, and is used as a dynamic scattering medium to verify the proposed method.

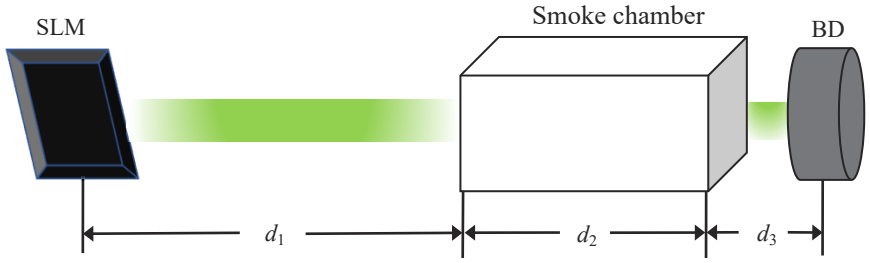

Fig. 4. A schematic of axial transmission distances in the designed free-space optical data transmission system: d_1, axial distance between spatial light modulator and front side of smoke chamber; d_2, length of smoke chamber; d_3, axial distance between back side of smoke chamber and single-pixel bucket detector.

Table 1. The parameters used in optical experiments.

Chambers with different volumes (cm^3)	Pumping time (s)	d_1 (cm)	d_3 (cm)	Total distance (cm)
$20\times30\times40$	7.5	82.5	2.5	105.0
$30\times30\times40$	11.25	72.5	2.5	105.0
$40\times30\times40$	15.0	62.5	2.5	105.0
$60\times30\times40$	22.5	42.5	2.5	105.0
$80\times30\times40$	30.0	22.5	2.5	105.0
$100\times30\times40$	37.5	2.5	2.5	105.0

3.2. Attenuation due to dynamic smoke

To study the impact of different smoke concentrations, a relationship between the collected light intensities and the concentrations of glycerol smoke can be obtained in real time by using optical thickness (OT). In this study, real-time OT in free-space optical transmission channel is calculated to describe concentration variations in the transmission channel based on Beer-Lambert law [41] defined by

$$I = I_0 e^{-OT}, \tag{13}$$

where I_0 denotes the recorded light power at the receiving end without smoke chamber in the free-space optical transmission system, and I denotes the recorded light power at the receiving end with smoke chamber placed in free-space optical transmission. Therefore, the OT can be calculated by

$$OT = -\ln\frac{I}{I_0}. \tag{14}$$

To eliminate measurement errors caused by the fluctuation of propagating wave, light intensities recorded at different time slots without the smoke chamber in the free-space optical transmission are used to calculate an average light power I_0 described by

$$I_0 = \frac{1}{V}\sum_{i=1}^{V} I_{0i}, \tag{15}$$

where V denotes the total measurement number, and I_{0i} denotes the light intensities recorded at the receiving end.

Optics EXPRESS

The light intensities recorded at different time slots are obtained and shown in Fig. 5(a), when smoke chambers with different volumes ($20\times30\times40$, $30\times30\times40$, $40\times30\times40$, $60\times30\times40$, $80\times30\times40$, and $100\times30\times40$ cm^3) are respectively used. The collected light intensities are small at the beginning, and increase with the sampling time and finally remain stable. Dynamic smoke pumped into the chamber has a high density at the beginning, and the propagating wave is strongly scattered through smoke chamber which results in only few light to be collected by the single-pixel bucket detector. It is also demonstrated in Fig. 5(a) that the light intensities recorded at the beginning are always at a low level, when the different smoke chambers are used. Due to precipitation and liquefaction process of the smoke, smoke concentration in the chambers decreases. In addition, the length of smoke chamber could affect the collected light intensities. The longer length of smoke chamber makes the collected light intensities smaller. Real-time OT values are further calculated based on Eq. (14) to describe the impact of dynamic smoke, and experimental results are shown in Fig. 5(b). As can be seen in Fig. 5(b), the trends are similar, when smoke chambers with different volumes are respectively used. The OT values are at a high level at the beginning, since smoke concentration in the chamber is at the largest level. As the sampling time increases, OT values decrease due to the existence of liquefaction and sedimentation of the smoke in the chamber.

3.3. Optical analog-data transmission

Due to dynamic smoke in the chamber, real-time OT values during optical transmission of different pixels of a signal are different. To better describe the OT in free-space optical data transmission through dynamic smoke, average optical thickness (AOT) is further calculated to measure the fluctuation. Each signal contains N pixels, and then in the proposed method the AOT can be calculated by

$$AOT = \frac{1}{2N}\sum_{i=1}^{2N} OT_i. \tag{16}$$

Four irregular analog signals are first encoded by using the proposed pixel-to-plane algorithm to generate a series of 2D arrays of random numbers, and then these 2D arrays of random numbers and the fixed reference pattern are alternately embedded into the amplitude-only spatial light modulator to be optically illuminated to propagate through dynamic smoke in Fig. 2 to verify the proposed method. Some typically experimental results are shown in Fig. 6, where the dot denotes original signal and the triangle denotes a signal retrieved at the receiving end. It is experimentally demonstrated in Figs. 6(a)–6(d) that the signals can be retrieved with high fidelity in the developed free-space optical data transmission through dynamic smoke by using the proposed method. To evaluate the signals retrieved at the receiving end, mean squared error (MSE) and peak signal-to-noise ratio (PSNR) are calculated by [42–46]

$$\mathrm{MSE} = \frac{1}{N}\sum_{i=1}^{N}(S_i - \tilde{S}_i)^2, \tag{17}$$

$$\mathrm{PSNR} = 10\log_{10}\frac{MAX_S^2}{\mathrm{MSE}}, \tag{18}$$

where S_i denotes original signal, $\tilde{S}_i$ denotes the retrieved signal, and MAX_S denotes the maximum pixel value of original signal. The AOT, MSE and PSNR values are calculated and given in Fig. 6, and low MSE values and high PSNR values of the retrieved signals are always obtained by using the proposed method. It is illustrated in Fig. 6 that the proposed method is feasible and effective.

Optical experiments are further conducted for a comparison, when the proposed method with and without the fixed reference pattern is applied in the free-space optical data transmission system through dynamic smoke. The experimental results are shown in Fig. 7. The measurement

Optics EXPRESS

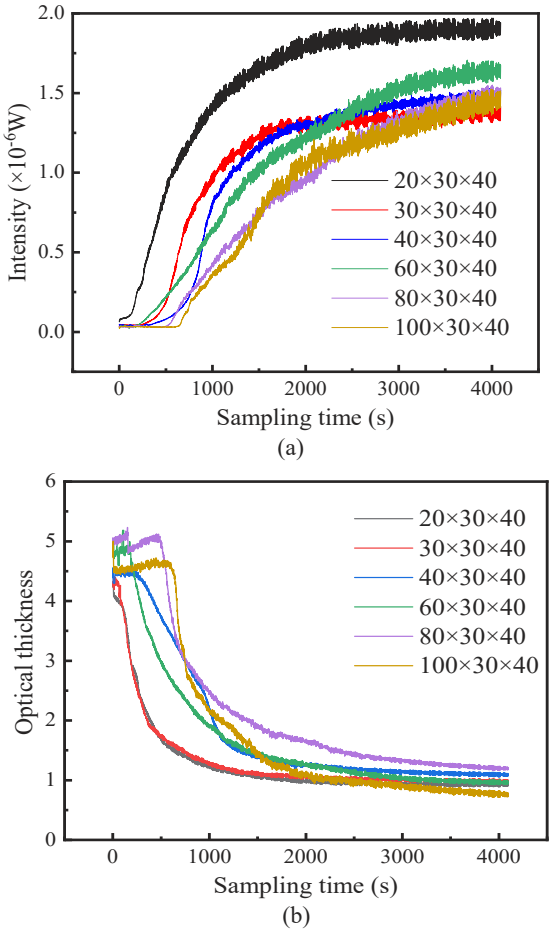

Fig. 5. (a) The light intensities recorded at the receiving end with the sampling time when the smoke chambers with different volumes ($20 \times 30 \times 40$, $30 \times 30 \times 40$, $40 \times 30 \times 40$, $60 \times 30 \times 40$, $80 \times 30 \times 40$, and $100 \times 30 \times 40$ cm^3) are respectively used, and (b) a relationship between the sampling time and real-time OT values when the smoke chambers with different volumes ($20 \times 30 \times 40$, $30 \times 30 \times 40$, $40 \times 30 \times 40$, $60 \times 30 \times 40$, $80 \times 30 \times 40$, and $100 \times 30 \times 40$ cm^3) are respectively used.

Optics EXPRESS

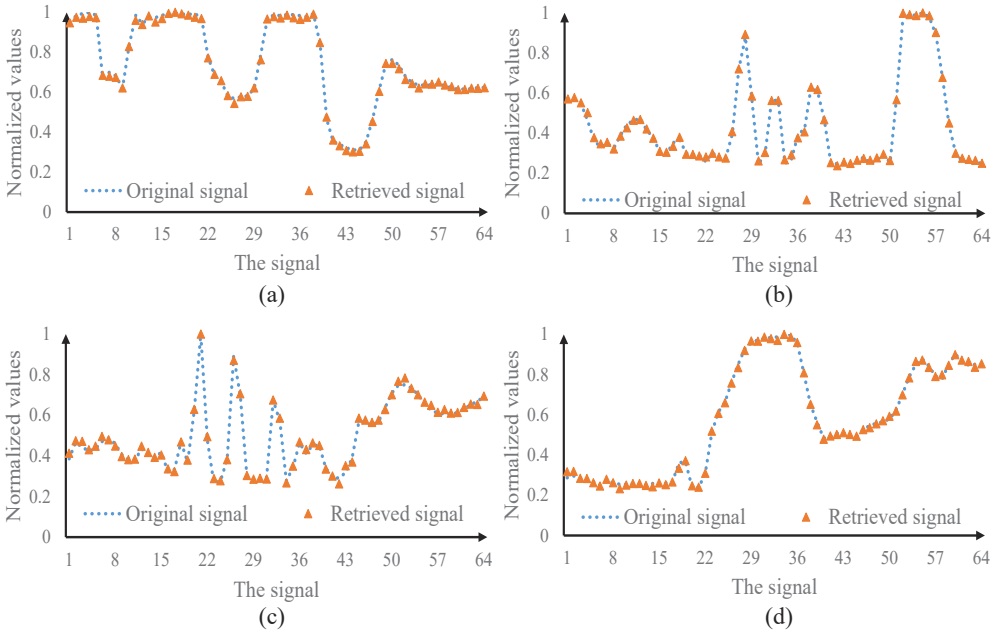

Fig. 6. (a)-(d) The signals experimentally retrieved at the receiving end with a smoke chamber of $80\times30\times40$ cm^3 and other experimental parameters in Table 1: the AOT in (a)-(d) is 1.58, 1.57, 1.63, and 1.59. PSNR values of the retrieved signals in (a)-(d) are 38.55 dB, 38.28 dB, 37.02 dB, and 39.94 dB, respectively. MSE values of the retrieved signals in (a)-(d) are 1.40×10^{-4}, 1.49×10^{-4}, 1.99×10^{-4}, and 1.01×10^{-4}, respectively.

sequence in Fig. 7 represents free-space optical information transmission of one fixed analog signal at different time slots. As can be seen in Fig. 7, when the AOT is at a high level (i.e., larger than 2.5), PSNR values of the retrieved signals with and without the reference pattern are small (i.e., lower than 30.0 dB). The large AOT values mean that smoke in the chamber has high density, and optical field information could be severely scattered. When the AOT decreases, PSNR values of the retrieved signals increase. In addition, PSNR values of the signals retrieved by using the proposed method with the fixed reference pattern are higher than those of the signals retrieved without the reference pattern. The fixed reference pattern is utilized in optical experiments to record real-time scaling factors, and then measurement errors caused by dynamic smoke can be corrected. The usage of a fixed reference pattern in the proposed method improves quality of the retrieved signals at the receiving end, when dynamic smoke environment is studied. It is also demonstrated that feasibility and effectiveness of the proposed high-fidelity free-space optical data transmission through dynamic smoke are verified.

The AOT is calculated to describe real-time destruction degree of optical field information in free-space optical data transmission through dynamic smoke. A relationship between the AOT and PSNR values of the retrieved signals is further obtained and shown in Fig. 8, when the smoke chambers with different volumes ($20\times30\times40$, $30\times30\times40$, $40\times30\times40$, $60\times30\times40$, $80\times30\times40$, and $100\times30\times40$ cm^3) are respectively used. As can be seen in Fig. 8, PSNR values of the retrieved signals decrease with the higher AOT. It is a downward trend, when the AOT is higher than 2.5. It is demonstrated in Fig. 8 that the retrieved signals are of high quality by using the proposed method when the AOT is lower than 2.5. The typically retrieved signals are shown in Figs. 9(a)–9(f), and the AOT and PSNR values of the retrieved signals are given in Figs. 9(a)–9(f). The label of x-axis in Figs. 9(a)–9(f) means the signal to be

Optics EXPRESS

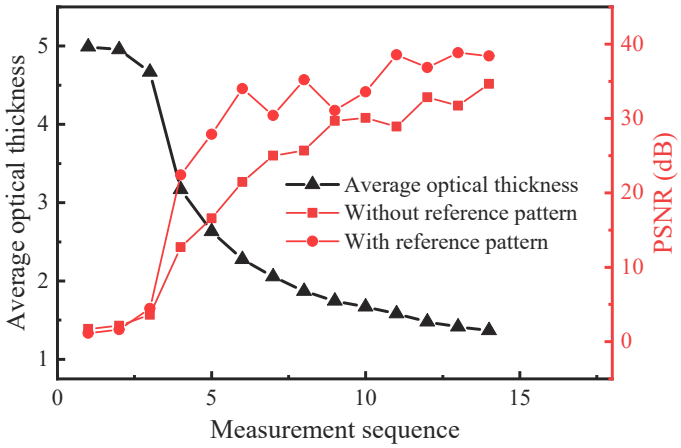

Fig. 7. A comparison of quality of the signals retrieved at the receiving end with and without the fixed reference pattern and the corresponding AOT values.

transmitted in dynamic smoke environment. Each transmitted signal has 64 pixels. As can be seen in Figs. 9(a)–9(f), the retrieved signals are of high fidelity by using the proposed method, when smoke chambers with different volumes are designed and used in the developed free-space optical data transmission through dynamic smoke. Based on the experimental results of irregular analog-signal transmission through dynamic smoke, binary signals can be retrieved with ultra-high fidelity when binary signals are tested based on the developed optical system. Binary signals are simpler to be transmitted compared with irregular analog signals, and the difference between transmitted binary signals and original binary signals is always 0 in the proposed method. Advantages of the proposed method are briefly described as follows: 1) Pixel-to-plane encoding algorithm is developed to transform each pixel of the signal into a 2D array of random numbers to be used as an information carrier. 2) Transmission errors induced by dynamic smoke are temporally corrected by using a fixed reference pattern. 3) A novel retrieval process is developed to realize high-fidelity signal transmission through dynamic smoke.

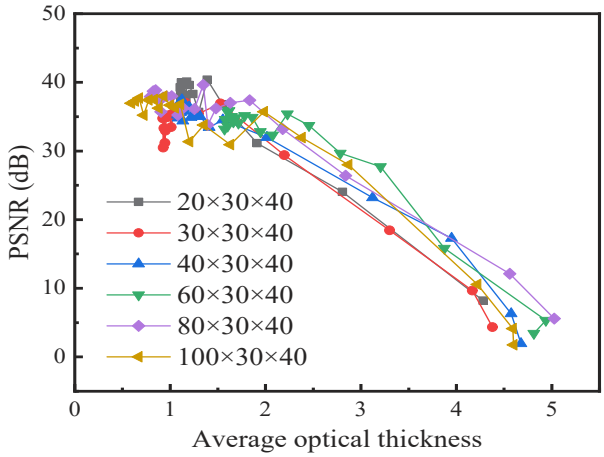

Fig. 8. A relationship between the AOT and the PSNR of the retrieved signals obtained when the smoke chambers with different volumes are respectively used. One fixed analog signal is repeatedly tested here.

Optics EXPRESS

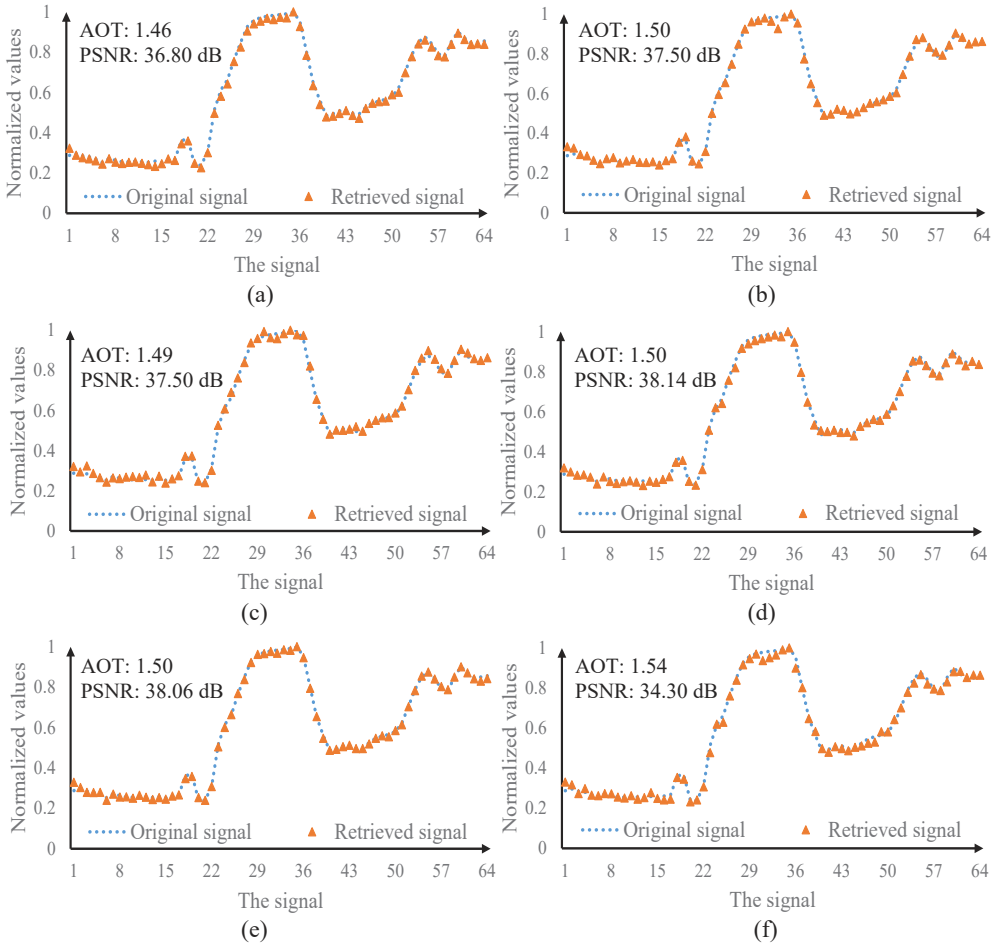

Fig. 9. (a)-(f) The signals retrieved at the receiving end using the proposed method when smoke chambers with different volumes (length d_2 of 20.0, 30.0, 40.0, 60.0, 80.0, and 100.0 cm) are respectively used.

4. Conclusion

A new approach is proposed to realize high-fidelity free-space optical data transmission through dynamic smoke using a series of 2D arrays of random numbers via pixel-to-plane encoding. A series of 2D arrays with random numbers are generated to be used as information carriers in the free-space optical data transmission channel. Transmission errors induced by dynamic smoke are temporally corrected using a fixed reference pattern. It is experimentally demonstrated that irregular analog signals can be retrieved with high fidelity at the receiving end, when the AOT in the free-space optical data transmission channel is lower than 2.5. It is expected that the proposed method could open up a novel research perspective for high-fidelity free-space optical data transmission through dynamic smoke.

Funding. GuangDong Basic and Applied Basic Research Foundation (2022A1515011858); Hong Kong Research Grants Council (C5011-19G, 15224921); Hong Kong Polytechnic University (G-R006, 4-R006, 1-W167, 1-W19E, 1-BD4Q).

Disclosures. The authors declare no conflicts of interest.

Optics EXPRESS

Data availability. Data underlying the results presented in this paper are not publicly available at this time but may be obtained from the authors upon reasonable request.

References

1. S. Ahmadzadeh, G. Parr, and W. Q. Zhao, "A Review on Communication Aspects of Demand Response Management for Future 5G IoT- Based Smart Grids," IEEE Access **9**, 77555–77571 (2021).
2. S. S. Oyewobi, K. Djouani, and A. M. Kurien, "A review of industrial wireless communications, challenges, and solutions: a cognitive radio approach," Trans. Emerg. Telecommun. Technol. **31**(9), e4055 (2020).
3. M. A. Khalighi and M. Uysal, "Survey on free space optical communication: a communication theory perspective," IEEE Commun. Surveys. Tuts. **16**(4), 2231–2258 (2014).
4. V. W. Chan, "Free-space optical communications," J. Lightwave Technol. **24**(12), 4750–4762 (2006).
5. G. Satat, M. Tancik, and R. Raskar, "Towards photography through realistic fog," in *2018 IEEE International Conference on Computational Photography (ICCP)*, (IEEE, 2018), pp. 1–10.
6. J. Duan, J. T. Zhan, S. Zhang, C. X. Zhao, J. Peng, Y. Lei, and Q. Fu, "Experiment of polarization transmission characteristics and polarization imaging in simulation smoke/fog environment," in *Annual Conference of the Chinese-Society-for-Optical-Engineering on Applied Optics and Photonics, China (AOPC)*, (Beijing, PEOPLES R CHINA, 2015), pp. 96740D.
7. S. Zheng, H. Wang, S. Dong, F. Wang, and G. Situ, "Incoherent imaging through highly nonstatic and optically thick turbid media based on neural network," Photonics Res. **9**(5), B220–B228 (2021).
8. K. Su, L. Moeller, R. B. Barat, and J. F. Federici, "Experimental comparison of performance degradation from terahertz and infrared wireless links in fog," J. Opt. Soc. Am. A **29**(2), 179–184 (2012).
9. M. Ijaz, Z. Ghassemlooy, H. Le-minh, S. Zvanovec, J. Perez, J. Pesek, and O. Fiser, "Experimental validation of fog models for FSO under laboratory controlled conditions," in *2013 IEEE 24th Annual International Symposium on Personal, Indoor, and Mobile Radio Communications (PIMRC)*, (IEEE, 2013), pp. 19–23.
10. Z. X. He, P. Zhang, D. Wu, X. J. Wu, S. He, J. Wei, X. Y. Gong, T. Wang, D. S. Wang, K. X. Han, S. F. Tong, and H. L. Jiang, "1.7 μm band modulated optical signal transmission through water fog using pump modulated Tm-doped fiber laser," in *Asia Communications and Photonics Conference (ACP)*, (Chengdu, PEOPLES R CHINA, 2019), pp. M4A–46.
11. S. Q. Hu, H. J. Liu, L. F. Zhao, and X. L. Bian, "The Link Attenuation Model Based on Monte Carlo Simulation for Laser Transmission in Fog Channel," IEEE Photon. J. **12**(4), 1–10 (2020).
12. Y. Guo, M. Kong, M. Sait, S. Marie, O. Alkhazragi, T. K. Ng, and B. S. Ooi, "Compact scintillating-fiber/450-nm-laser transceiver for full-duplex underwater wireless optical communication system under turbulence," Opt. Express **30**(1), 53–69 (2022).
13. C. Shen, Y. Guo, H. M. Oubei, T. K. Ng, G. Liu, K. H. Park, K. T. Ho, M. S. Alouini, and B. S. Ooi, "20-meter underwater wireless optical communication link with 1.5 Gbps data rate," Opt. Express **24**(22), 25502–25509 (2016).
14. Z. Ghassemlooy, H. Le Minh, S. Rajbhandari, J. Perez, and M. Ijaz, "Performance analysis of ethernet/fast-ethernet free space optical communications in a controlled weak turbulence condition," J. Lightwave Technol. **30**(13), 2188–2194 (2012).
15. J. Perez, Z. Ghassemlooy, S. Rajbhandari, M. Ijaz, and H. L. Minh, "Ethernet FSO communications link performance study under a controlled fog environment," IEEE Commun. Lett. **16**(3), 408–410 (2012).
16. M. Ijaz, Z. Ghassemlooy, J. Pesek, O. Fiser, H. L. Minh, and E. Bentley, "Modeling of fog and smoke attenuation in free space optical communications link under controlled laboratory conditions," J. Lightwave Technol. **31**(11), 1720–1726 (2013).
17. B. R. Babaria, T. L. Alvarez, M. T. Bergen, and R. J. Servatius, "Transmission of light in a synthetic fog medium," in *IEEE 30th Annual Northeast Bioengineering Conference*, (Western New England Coll, Springfield, MA, 2004), pp. 23–24.
18. P. Lin, T. Wang, W. Ma, Q. Yang, and Z. Liu, "Transmission characteristics of 1.55 and 2.04 μm laser carriers in a simulated smoke channel based on an actively mode-locked fiber laser," Opt. Express **28**(26), 39216–39226 (2020).
19. C. Zhang, J. Zhang, X. Wu, and M. Huang, "Numerical analysis of light reflection and transmission in poly-disperse sea fog," Opt. Express **28**(17), 25410–25430 (2020).
20. M. Ijaz, Z. Ghassemlooy, H. L. Minh, S. Rajbhandari, and J. Perez, "Analysis of fog and smoke attenuation in a free space optical communication link under controlled laboratory conditions," in *2012 International Workshop on Optical Wireless Communications*, (IEEE, 2012), pp. 1–3.
21. P. Duthon, M. Colomb, and F. Bernardin, "Light Transmission in Fog: The Influence of Wavelength on the Extinction Coefficient," Appl. Sci. **9**(14), 2843 (2019).
22. X. X. Chen and Z. S. Wu, "Transmission Characteristics of Polarized Light in Low Visibility Fog," in *12th International Symposium on Antennas, Propagation and Electromagnetic Theory (ISAPE)*, (Hangzhou, PEOPLES R CHINA, 2018), pp. 1–5.
23. L. Ma, C. Wang, and L. Liu, "Polarized radiative transfer in dense dispersed media containing optically soft sticky particles," Opt. Express **28**(19), 28252–28268 (2020).
24. X. Zeng, X. Chen, Y. Li, and Q. Xiangnan, "Polarization enhancement of linearly polarized light through foggy environments at UV–NIR wavelengths," Appl. Opt. **60**(26), 8103–8108 (2021).

Optics EXPRESS

25. S. Zhang, J. T. Zhan, Q. Fu, J. Duan, Y. C. Li, and H. L. Jiang, "Propagation of linear and circular polarization in a settling smoke environment: theory and experiment," Appl. Opt. **58**(17), 4687–4694 (2019).
26. X. W. Zeng, J. K. Chu, W. D. Cao, W. D. Kang, and R. Zhang, "Visible-IR transmission enhancement through fog using circularly polarized light," Appl. Opt. **57**(23), 6817–6822 (2018).
27. S. Zhang, J. Zhan, Q. Fu, J. Duan, Y. Li, and H. Jiang, "Effects of environment variation of glycerol smoke particles on the persistence of linear and circular polarization," Opt. Express **28**(14), 20236–20248 (2020).
28. B. Z. Bentz, B. J. Redman, J. D. van der Laan, K. Westlake, A. Glen, A. L. Sanchez, and J. B Wright, "Light transport with weak angular dependence in fog," Opt. Express **29**(9), 13231–13245 (2021).
29. B. Wu, B. Marchant, and M. Kavehrad, "Channel modeling of light signals propagating through a battlefield environment: analysis of channel spatial, angular, and temporal dispersion," Appl. Opt. **46**(25), 6442–6448 (2007).
30. P. Qiu, G. Cui, Z. Qian, S. Zhu, X. Shan, Z. Zhao, X. Zhou, X. Cui, and P. Tian, "4.0 Gbps visible light communication in a foggy environment based on a blue laser diode," Opt. Express **29**(9), 14163–14173 (2021).
31. M. S. Awan, P. Brandl, E. Leitgeb, F. Nadeem, L. Csugai-Horvath, and R. Nebuloni, "Transmission of High Data Rate Optical Signals in Fog and Snow Conditions," in *1st International Conference on Wireless Communication, Vehicular Technology, Information Theory and Aerospace and Electronic Systems Technology*, (Aalborg, DENMARK, 2009), pp. 702–706.
32. J. Perez, S. Zvanovec, Z. Ghassemlooy, and W. O. Popoola, "Experimental characterization and mitigation of turbulence induced signal fades within an ad hoc FSO network," Opt. Express **22**(3), 3208–3218 (2014).
33. J. Libich, J. Perez, S. Zvanovec, Z. Ghassemlooy, R. Nebuloni, and C. Capsoni, "Combined effect of turbulence and aerosol on free-space optical links," Appl. Opt. **56**(2), 336–341 (2017).
34. A. Almogahed, A. Amphawan, F. Mohammed, A. Alawadhi, and C. Yuen, "Performance improvement of mode division multiplexing free space optical communication system through various atmospheric conditions with a decision feedback equalizer," Cogent Eng. **9**(1), 2034268 (2022).
35. A. Almogahed, A. Amphawan, and Y. Fazea, "Mitigation of atmospheric turbulences using mode division multiplexing based on decision feedback equalizer for free space optics," J. Opt. Commun. **41**(2), 185–193 (2020).
36. D. Shah and D. Kothari, "Mitigation of fog and rain effects in free-space optical transmission using combined diversity," in *2nd International Conference on Computer and Communication Technologies*, (CMR Tech Campus, Hyderabad, INDIA, 2015), pp. 725–733.
37. B. Judkewitz, R. Horstmeyer, I. M. Vellekoop, I. N. Papadopoulos, and C. Yang, "Translation correlations in anisotropically scattering media," Nat. Phys. **11**(8), 684–689 (2015).
38. E. Tajahuerce, V. Durán, P. Clemente, E. Irles, F. Soldevila, P. Andrés, and J. Lancis, "Image transmission through dynamic scattering media by single-pixel photodetection," Opt. Express **22**(14), 16945–16955 (2014).
39. E. Kristensson, J. Bood, M. Aldén, E. Nordström, J. Zhu, S. Huldt, P. E. Bengtsson, H. Nilsson, E. Berrocal, and A. Ehn, "Stray light suppression in spectroscopy using periodic shadowing," Opt. Express **22**(7), 7711–7721 (2014).
40. E. Kristensson, A. Ehn, and E. Berrocal, "High dynamic spectroscopy using a digital micromirror device and periodic shadowing," Opt. Express **25**(1), 212–222 (2017).
41. H. K. Hughes, "Beer's law and the optimum transmittance in absorption measurements," Appl. Opt. **2**(9), 937–945 (1963).
42. M. Dehshiri, S. G Sabouri, and A. Khorsandi, "Structural similarity assessment of an optical coherence tomographic image enhanced using the wavelet transform technique," J. Opt. Soc. Am. A **38**(1), 1–9 (2021).
43. Z. Pan, Y. Xiao, L. Zhou, Y. Cao, M. Yang, and W. Chen, "Non-line-of-sight optical information transmission through turbid water," Opt. Express **29**(24), 39498–39510 (2021).
44. Y. Xiao, L. Zhou, and W. Chen, "Wavefront control through multi-layer scattering media using single-pixel detector for high-PSNR optical transmission," Opt. Lasers Eng. **139**, 106453 (2021).
45. Y. Cao, Y. Xiao, Z. Pan, L. Zhou, and W. Chen, "Direct generation of 2D arrays of random numbers for high-fidelity optical ghost diffraction and information transmission through scattering media," Opt. Lasers Eng. **158**, 107141 (2022).
46. Z. Pan, Y. Xiao, Y. Cao, L. Zhou, and W. Chen, "Optical analog-signal transmission and retrieval through turbid water," Appl. Opt. **60**(34), 10704–10713 (2021).